# CO2 capture in a hollow fiber membrane contactor coupled with ionic liquid: Influence of membrane wetting and process parameters

Sohaib Qazi, Lucía Gómez-Coma, Jonathan Albo, Stéphanie Druon-Bocquet,
Angel Irabien, José Sanchez-Marcano

**CO$_2$ Capture in a Hollow Fiber Membrane Contactor Coupled with Ionic Liquid: Influence of Membrane Wetting and Process Parameters**

**Sohaib Qazi[1], Lucía Gómez Coma[2], Jonathan Albo[2], Stéphanie Druon-Bocquet[1], Angel Irabien[2], José Sanchez-Marcano[1]**

1 : Institut Européen des Membranes, IEM – UMR 5635, CNRS, ENSCM, Université de Montpellier, Montpellier, France.

2 : Chemical and Biomolecular Engineering Department, Universidad de Cantabria, Av. Los Castros, 39005 Santander, Spain.

**Abstract**

The present work demonstrates the potential of coupling ionic liquid 1-ethyl-3-methylimidazolium ethylsulfate ([emim][EtSO$_4$]) and hollow fiber membrane contactors for post-combustion CO$_2$ capture. CO$_2$ absorption experiments in counter-current configuration were carried out, followed by a comprehensive two-dimensional dynamic modeling based on steady state and pseudo-steady state operating modes. The model considers the level of wetting of porous hollow fibers. An overall mass transfer coefficient of 3.99 10$^{-5}$ m.s$^{-1}$ and CO$_2$ flux 6.1 10$^{-5}$ mol.m$^{-2}$.s$^{-1}$ were obtained for 100 ml.min$^{-1}$ of gas flowing inside the fibers. The model predicted the effects of membrane wetting, porosity, tortuosity, module length, fiber inner diameter, gas and absorbent flow rates. Membrane wetting has a noteworthy effect on CO$_2$ capture efficiency. A smaller amount of wetting can cause a huge resistance in CO$_2$ transport through the membrane. The separation efficiency was enhanced by using membranes with high porosity and low tortuosity and decreased by enhancing the gas flow rate and absorbent flow rate reduction. CO$_2$ capture is enhanced by increasing module length and reduction of inner diameter of fibers.

**Key Words:** CO$_2$ Capture, Membrane Contactor, Ionic Liquid, Membrane Wetting, Modelling

**Nomenclature**

| | |
|---|---|
| $A$ | Area $(m^2)$ |
| $C$ | Concentration $(mol.\,m^{-3})$ |
| $D$ | Diffusivity $(m^2.\,s^{-1})$ |
| $d_p$ | Membrane pore diameter $(m)$ |
| $H$ | Henry law solubility constant $(Pa^{-1})$ |
| $j$ | Molar flux $(mol.\,m^{-2}.\,s^{-1})$ |
| $K$ | Overall mass transfer coefficient $(m.\,s^{-1})$ |
| $L$ | Length of membrane $(m)$ |
| $\acute{m}$ | Distribution factor of $CO_2$ (-) |
| $M_w$ | Molar weight $(kg.\,mol^{-1})$ |
| $n$ | Number of fibers |
| $P$ | Pressure $(Pa)$ |
| $Q$ | Volumetric flowrate $(m^3.\,s^{-1})$ |
| $r$ | Radial coordinate $(m)$ |
| $r_1$ | Inner radius of the tube $(m)$ |
| $r_2$ | Outer radius of the tube $(m)$ |
| $r_3$ | Radius of the free surface $(m)$ |
| $R$ | Module inner radius $(m)$ |
| $\acute{R}$ | Reaction rate $(mol.\,m^{-3}.\,s^{-1})$ |
| $\mathfrak{R}$ | Perfect gas constant $(J.\,mol^{-1}.\,K^{-1})$ |
| $t$ | Time $(s)$ |
| $T$ | Temperature $(K)$ |
| $u$ | Average velocity $(m.\,s^{-1})$ |
| $U$ | Velocity $(m.\,s^{-1})$ |
| $v$ | Molar volume $(cm^3.\,mol^{-1})$ |
| $V$ | Volume $(m^3)$ |
| $z$ | Axial coordinate $(m)$ |


**Subscripts**

| | |
|---|---|
| $CO_2$ | Carbon dioxide |
| exp | Experimental |

| | |
|---|---|
| $g$ | Gas |
| $i$ | Component $i$ |
| $IL$ | Ionic Liquid |
| in | Inlet |
| $l$ | Liquid |
| M | Membrane |
| $N_2$ | Dinitrogen |
| out | Outlet |
| S | Shell |
| T | Tube |
| Tank | In the recycling tank |
| Z | Axial |

## Greek Letters

| | |
|---|---|
| $\mu$ | Viscosity ($cP$) |
| $\Theta$ | Contactor volumetric void fraction (-) |
| $\rho$ | Density ($kg.m^{-3}$) |
| $\bar{\upsilon}$ | Atomic diffusion volume (-) |
| $\varepsilon$ | Membrane porosity (-) |
| $\epsilon$ | Removal efficiency ($\%$) |
| $\tau$ | Membrane tortuosity (-) |
| $\mathcal{T}$ | Ionic liquid residence time ($s$) |
| $\delta$ | Membrane thickness ($m$) |
| $\varphi_v$ | $CO_2$ amount in feed gas (% vol) |
| $\theta$ | Cylindrical coordinate (rad) |
| $\Upsilon$ | Surface Tension (mN.m$^{-1}$) |

# 1    Introduction

Anthropogenic increase in emission of carbon dioxide ($CO_2$), which is a major contributor to global warming and climate change, has driven world's attention towards $CO_2$ capture and storage. Due to the world's dependency on fossil fuels, $CO_2$ emission is increasing by 6 % every year [1–3]. Generally, three different carbon capture strategies are being studied to mitigate $CO_2$ emissions: oxyfuel-combustion, pre-combustion and post-combustion separation processes. Post-combustion capture is the most effective and feasible way for $CO_2$ mitigation because this separation process can be applied to all combustion processes and can be retrofitted to existing power and industrial plants [3,4].

There are various technologies used for $CO_2$ capture including membranes, packed towers, spray towers, absorption columns and other conventional industrial methods [5]. Hollow fiber membrane contactors (HFMCs) are a hybrid technology that combines both membrane and absorption and can achieve dispersion free gas/liquid and liquid/liquid mass transfers. HFMCs are more advantageous over other conventional columns due to its larger and constant interfacial area per unit volume, absence of flooding, foaming and entrainment, independent control of flow rates, easy scale up and modularity. An HFMC provides 30 times more interfacial area compared to other conventional absorbers. A major disadvantage in HFMC is the additional mass transfer resistance due to the membrane especially in wetting mode [4,6–8]. Another possible problem with HFMCs operation is that flue gases contain a non-negligible amount of water vapor. Pourafshari Chenar et al. [9] investigated this effect (gases at 60 % of relative humidity) on $CO_2/CH_4$ permeance in hollow fiber membranes. Results revealed that there was a decline in the $CO_2$ and $CH_4$ permeance due to the presence of water vapor. On the contrary, a very recent study by Villeneuve et al. [10] showed that water vapor presence has no significant effect on $CO_2$ absorption in HFMCs. For this purpose, laboratory scale $CO_2$ gas liquid absorption experiments were carried out with 30 wt% aqueous MEA solution in HFMC with overheated (~50 $^{\circ}$C) and water saturated (~80 % relative humidity) feed gas on the lumen side. To study the process with in the industrial frame, a one-dimensional adiabatic model adopting commercial simulation environment was implemented for $CO_2$ absorption in MEA. Carbon capture efficiencies nearly remained same for humid and dry gas operations. The results showed that water vapor condensation occurs only in the gas side or it may occur on membrane-gas surface but not inside membrane pores. The humid gas significantly led to higher pressure drop. A higher proportionality factor (about 40 %) was observed between pressure drop and gas flowrate for humid feed gas.

Various chemical and physical absorbents have been used in HFMCs for $CO_2$ capture. Amines, aqueous solvents, enzyme solutions, ionic liquids (ILs) and blends of physical and/or chemical absorbents have been investigated [4,11]. The concept of using ILs for $CO_2$ capture is gaining interest due to its unique characteristics [12–14]. ILs, due to their distinctive properties such as, thermal stability, wide liquid range, negligible volatility, tunable physico-chemical character, tailorable structures and high solubility, are driving researchers attention from the past few decades [1,12,15–18]. Various ILs have been used by researchers for $CO_2$ capture. Gomez-Coma et al. [19] investigated the temperature influence on non-dispersive absorption of $CO_2$ in polysulphone HFMC using 1-Ethyl-3-methylimidazolium acetate ([emim][Ac]). The author also used various ratios of aqueous solution of [emim][Ac] to investigate its effect on $CO_2$ capture efficiency [20]. Lu et al [21] studied the membrane absorption coupling process for $CO_2$ absorption and absorbent regeneration with two ILs, 1-butyl-3-methyl-imidazolium tetrafluoroborate, [bmim][$BF_4$] (as physical absorbent) and 1-(3-aminopro pyl)-3-methyl-imidazolium tetrafluoroborate, [apmim][$BF_4$]  (as chemical absorbent). The absorption process was investigated for both open loop and close loop modes. Wetting of the mesoporous membrane was not taken into account due to high surface

tension of the absorbents and use of fresh hydrophobic membrane. The aqueous [apmim][BF$_4$] was able to maintain high membrane flux and showed high $CO_2$ loading capacity at atmospheric pressure, compared to aqueous [bmim][BF$_4$]. Dai et al [22] investigated the compatibility and stability of six different porous and non-porous polymeric HFMCs using IL 1-Butyl-3-methylimidazolium tricyanomethanide [bmim][TCM] as absorbent for $CO_2$. The study has reported an enhanced mass transfer flux with increase in gas flowrate for both porous and nonporous membranes. In another study [23] the author has used the IL [bmim][TCM] for $CO_2$ capture in porous tubular membrane contactor. An increase in $CO_2$ flux and experimental mass transfer coefficients have been reported with increase in gas flowrate. A decrease of 22% in overall mass transfer coefficient has been reported for only 1 % wetting of the membrane.

Simulation is a potential tool for easy scale up and reduction of optimization cost of an available design. Many researchers have focused on modelling and simulation of $CO_2$ capture in HFMCs with conventional absorbents. However, there is a limited literature available on modelling and simulation of $CO_2$ absorption in HFMCs with ILs [2,6]. Thus far, many researchers have worked on simulation of post-combustion $CO_2$ capture. To the best of the authors' knowledge, there is no available report on simulation of $CO_2$ capture in HFMCs using ILs as absorbent, considering partially wetted and fully wetted conditions, with dynamic modelling for recycled absorbent.

This work focuses on both experimental and modelling studies of $CO_2$ absorption in coupled system of an IL and a HFMC. A polypropylene membrane contactor was used due to its hydrophobicity and resistance to dissolve in common solvents. IL 1-Ethyl-3-methylimidazolium ethylsulfate [emim][EtSO$_4$] was used as an absorbent for $CO_2$ due to its high $CO_2$ solubility, physical absorption behavior for $CO_2$ and green nature. A comprehensive two-dimensional (2D) dynamic model was developed to study the mass transport of $CO_2$ and separation behavior of $CO_2$/$N_2$ mixture in both steady state and pseudo-steady state modes of operation. The model considers non-wetted, partially wetted and fully wetted conditions. Results from the model were validated with experimental data. $CO_2$ absorption behavior and setup performance were studied in terms of separation efficiency, $CO_2$ flux and overall mass transfer coefficient. In the simulation, effects of membrane configuration (porosity, tortuosity, module's length and fiber inner diameter) on $CO_2$ removal efficiency were studied. A detailed concentration profile was investigated in all wetted and non-wetted conditions. Furthermore, the effect of operating conditions (gas flow rate, absorbent flow rate and temperature) on $CO_2$ removal efficiency was also studied.


## 2    Experimental

### 2.1    Material
Carbon dioxide (99.7 %) and Nitrogen (99.9 %) were purchased from Air Liquide, Spain. A parallel configuration hydrophobic HFMC (X50 module) was supplied by Liqui-Cel [TM], USA. Modules were manufactured with mesoporous polypropylene hollow fiber membranes (0.04 µm) potted with polyurethane. Configurations of the module are presented in table 1. IL 1-Ethyl-3-methylimidazolium ethylsulfate [emim][EtSO$_4$] with more than 95 % purity was purchased from Sigma-Aldrich.

### 2.2    Methods
A coupled HFMC-IL setup suitable for low temperature and pressure applications was used to investigate the absorption behavior of $CO_2$ at various conditions. The setup is illustrated in figure 1. Operating conditions for the absorption process are presented in table 2.

The feed gas mixture contains $CO_2$, 15 % vol. and $N_2$ (rest to balance). The gas flowing through the fibers of the module was measured and controlled by gas mass flowmeters (Alicat scientific, MC–gas mass flow controller, Spain). IL was pumped from a reservoir, through the shell side of the module by a digital gear pump (Cole-Parmer Gear Pump System, Benchtop Digital Drive, 0.017 mL/rev, 220 VAC, Spain) to maintain a constant flowrate and avoid fluctuations. The absorption setup along with the IL reservoir were kept in oven to maintain isothermal conditions during the absorption. Carbon dioxide concentration in the inlet and outlet gas stream was measured by a $CO_2$ analyzer (Geotech, G110 0-100%, UK).

The gas mixture (which flows in open loop) was introduced through the lumen (inner) side of the fibers in counter current mode at nearly atmospheric pressure. The IL was recirculated from a reservoir in a closed loop. Liquid side pressure was kept slightly higher than gas side to avoid penetration of gas into the liquid side. Experiments were performed inside an oven to maintain controlled temperature environment and isothermal conditions during the absorption. IL during recirculation absorbs $CO_2$ from $CO_2/N_2$ mixture. $CO_2$ concentration in the outlet gas stream was continuously measured by $CO_2$ analyzer. The setup was investigated against various operating conditions.

The $CO_2$ absorption flux and experimental overall mass transfer coefficient can be calculated by the following equations.

$$j_{CO_2} = \frac{Q_{g\_in}C_{g\_in} - Q_{g\_out}C_{g\_out}}{A} = K_{exp}\Delta C_g \tag{1}$$

$$\Delta C_g = \frac{C_{g\_in} - C_{g\_out}}{\ln\left(\frac{C_{g\_in}}{C_{g\_out}}\right)} \tag{2}$$

Where $Q_{g\_in}$ and $Q_{g\_out}$ represent gas side inlet and outlet flow rates $(m^3.s^{-1})$, respectively, $C_{g\_in}$ and $C_{g\_out}$ are gas side inlet and outlet concentrations $(mol.m^{-3})$ of $CO_2$, respectively. $C_{g\_out}$ value was noted from the gas analyzer. $\Delta C_g$ represents logarithmic mean of driving force based on gas phase concentration.
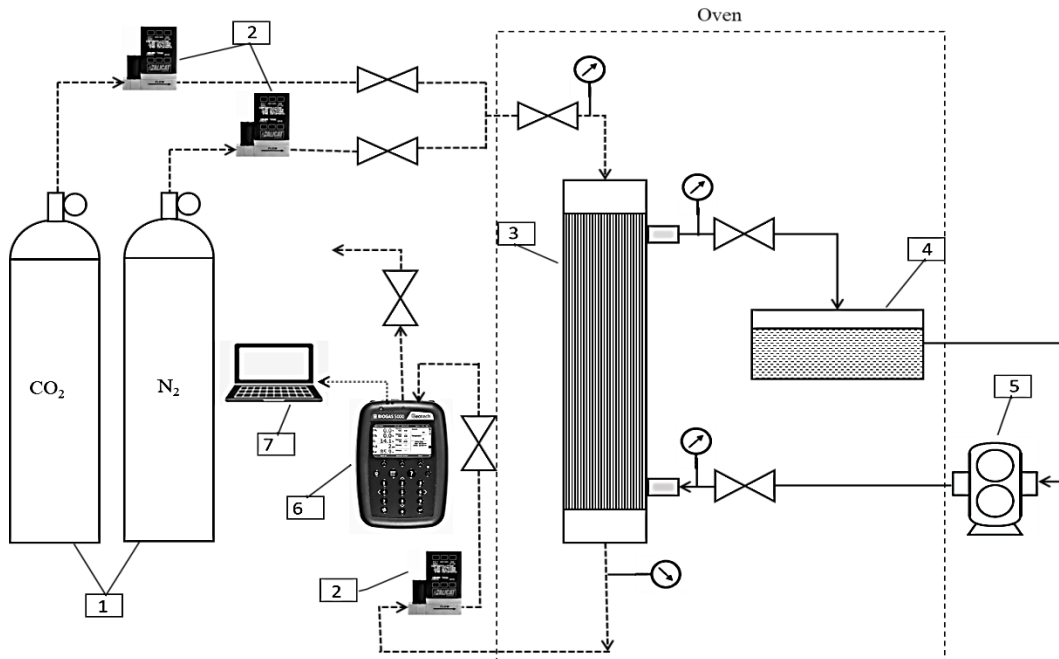
**Figure 1** Schematic representation of the experimental setup; 1-$N_2$ and $CO_2$ gas cylinders, 2-Gas flowmeters, 3-HFMC module, 4-IL Reservoir, 5-Gear Pump, 6-$CO_2$ analyzer, 7-Computer connected to $CO_2$ analyzer.

**Table 1** Specification of the membrane module.

| Parameter | Value | unit |
|---|---|---|
| Membrane material | Polypropylene | - |
| Inside radius of the tube ($r_1$) | $1.1 \times 10^{-4}$ | m |
| Outside radius of the tube ($r_2$) | $1.5 \times 10^{-4}$ | m |
| Membrane thickness ($\delta$) | $0.4 \times 10^{-4}$ | m |
| Length of the contactor (L) | 0.115 | m |
| Number of fibers (n) | 2300 | - |
| Membrane pore diameter($d_p$) | 0.04 | µm |
| Effective inner membrane area (A) | 0.18 | $m^2$ |
| Porosity ($\varepsilon$) | 40 | % |
| Packing factor | 0.39 | - |
| Tortuosity ($\tau$)[a] | 2.5 | - |

[a] Assumed as $1/\varepsilon$

**Table 2** Operating conditions.

| Parameter/Property | Value | Unit |
|---|---|---|
| Ionic liquid | [emim] [EtSO$_4$] ≥ 95% | - |
| $\varphi_v$ | 15 | Vol % |
| T | 291 | K |
| $Q_g$ | 50-100 | ml.min$^{-1}$ |
| $Q_{IL}$ | 60 | ml.min$^{-1}$ |
| $P_{gin}$ | 0.103 | MPa |
| $P_{Lin}$ | 0.131 | MPa |

## 3    Model development

A comprehensive 2D model is presented (for the experimental setup in section 2.2) to study the mass transfer of $CO_2$ in porous hydrophobic polypropylene HFMC by solving the continuity equations for the three domains: the gas side, porous membrane and absorbent side. Feed mixture containing $CO_2$ and $N_2$ is allowed to flow in the inner side of the fibers considering a fully developed laminar parabolic velocity profile. 1-Ethyl-3-methylimidazolium ethylsulfate [emim][EtSO$_4$] used as an absorbent, can flow counter currently through the shell side (outer side) as shown in figure 2. Figure 2(a) shows a single hollow fiber with arbitrary shell predicted by Happel's model [24]. A portion of the fiber along with arbitrary shell is shown in figure 2(b). Process parameters are listed in table 3.
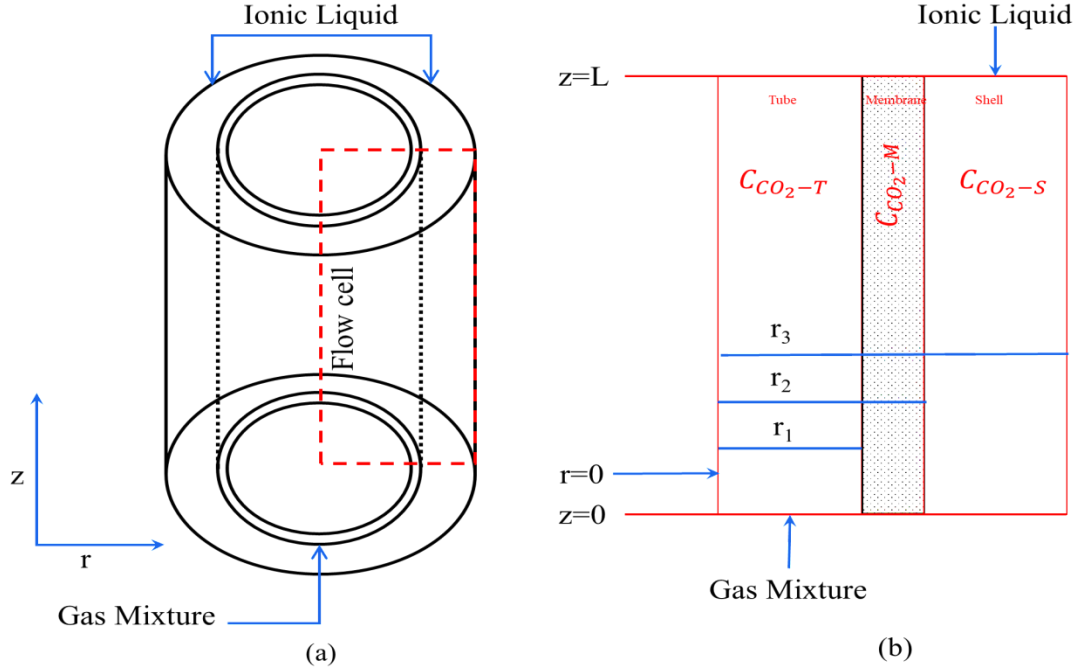
**Figure 2** Schematic diagram of single hollow fiber and section used for model development.

**Table 3** Properties and process parameters.

| Parameter/Property | Value | Unit | Reference |
|---|---|---|---|
| $\mu_{IL}$; 291 K | 123.5 | mPa.s | [25] |
| $\rho_{IL}$; 291 K | 1.241 | g.cm$^{-3}$ | [25] |
| $\Upsilon_{IL}$; 298 K | 47.31 | mN.m$^{-1}$ | [26] |
| $D_{CO_2\text{-}l}$; 291 K | 2.88 10$^{-6}$ | cm$^2$. s$^{-1}$ | Equation 6 |
| $D_{CO_2\text{-}g}$; 291 K | 1.55 10$^{-1}$ | cm$^2$. s$^{-1}$ | Equation 13 |
| $D_{CO_2\text{-}Mg}$; 291 K | 2.48 10$^{-2}$ | cm$^2$. s$^{-1}$ | Equation 17 |
| H ; 303 K | 1.611 | MPa$^{-1}$ | [27] |

### 3.1 Assumptions

The following assumptions were made in order to simplify the problem.

- Countercurrent mode, gas in the tube and liquid in the shell.
- Steady state and isothermal conditions in the HFMC module (unless mentioned).
- The tank is considered as a perfect stirred tank.
- Laminar flow conditions for both gas and absorbent.
- Application of Henry law on gas-liquid interface.
- Axial radial concentration gradient.
- Membrane does not provide selectivity.

- Physical absorption (no chemical reaction considered).

## 3.2  Transport equations

A schematic diagram of the counter current flow of absorbent (shell side) and gas (tube side) is shown in figure 2. The continuity equation for each section is expressed as:

$$\frac{\partial C_i}{\partial t} = -\nabla.C_i U - \nabla.j_i + \acute{R}_i \tag{3}$$

Where $C_i(mol.m^{-3})$, $U\ (ms^{-1})$, $j_i\ (mol.m^{-2}.s^{-1})$, $\acute{R}_i\ (mol.m^{-3}.s^{-1})$ and $t\ (s)$ are the concentration, velocity, molar flux, reaction rate and time, respectively. Fick's law of diffusion is used for the determination of fluxes [28]. Equation (3) is more simplified in later sections for steady state and no reaction conditions.

### 3.2.1  Shell side

Based on the above assumptions the transport of $CO_2$ in shell side can be expressed as below:

$$\frac{\partial C_{CO_2-S}}{\partial t} + D_{CO_2-S}\left[\frac{\partial^2 C_{CO_2-S}}{\partial r^2} + \frac{1}{r}\frac{\partial C_{CO_2-S}}{\partial r} + \frac{\partial^2 C_{CO_2-S}}{\partial z^2}\right] = U_{z-S}\frac{\partial C_{CO_2-S}}{\partial z} \tag{4}$$

For steady state the equation becomes as;

$$D_{CO_2-S}\left[\frac{\partial^2 C_{CO_2-S}}{\partial r^2} + \frac{1}{r}\frac{\partial C_{CO_2-S}}{\partial r} + \frac{\partial^2 C_{CO_2-S}}{\partial z^2}\right] = U_{z-S}\frac{\partial C_{CO_2-S}}{\partial z} \tag{5}$$

Where $D_{CO_2-S}(m^2.s^{-1})$, $C_{CO_2-S}\ (mol.m^{-3})$ and $U_{z-S}\ (m.s^{-1})$ denote the $CO_2$ diffusivity, $CO_2$ concentration and liquid velocity in the shell, respectively.

Gas diffusion coefficient in ionic liquids can be described by the following equation developed by Morgan et al. [29]:

$$D_{CO_2-l} = 2.66\ 10^{-3}\frac{1}{\mu_{IL}^{0.66}v_{CO_2}^{1.04}} \tag{6}$$

Where $\mu_{IL}(cP)$ and $v_{CO_2}(cm^3.mol^{-1})$ are viscosity of IL and molar volume of $CO_2$.

An increase in temperature effectively reduces viscosity of IL which causes an increase in diffusivity of $CO_2$ in IL at relatively high temperatures. Equation 6 has been verified in various studies by comparing the diffusivities from correlation with experimental diffusivities [30,31].

Happel's model is used to predict the velocity profile in the shell side [24]:

$$U_{z-S}(r) = 2u_{IL}[1 - (\frac{r_2}{r_3})^2][\frac{(r/r_3)^2 - (r_2/r_3)^2 + 2\ln(r_2/r)}{3 + (r_2/r_3)^4 - 4(r_2/r_3)^2 + 4\ln(r_2/r_3)}] \tag{7}$$

Where $u_{IL}$, $r_2$ and $r_3$ are average velocity of absorbent in the shell, outer radius of fiber and radius of free surface. Radius of free surface can be predicted by the following equation:

$$r_3 = (\frac{1}{1-\theta})^{1/2}r_2 \tag{8}$$

Where Θ is the contactor volumetric void fraction which is described by the following equation:

$$1 - \Theta = \frac{n r_2^2}{R^2}$$ (9)

In the above equation $n$ is the number of fibers and $R$ is the module inner radius.

Boundary conditions are listed in table 4.

As the model considers Henry's law for the gas liquid interface, a dimensionless Henry constant is used as a distribution factor across gas liquid interface. Henry's solubility constant for $CO_2$ solubility in [emim] [EtSO₄] is used to find the dimensionless distribution factor [27,32]. The constant is temperature dependent and increases simultaneously with temperature for [emim] [EtSO₄]. Increase in the Henry's constant shows that solubility of $CO_2$ decreases for the IL, with temperature enhancement. The distribution factor ṁ is expressed by the following equation [33]:

$$ṁ = \frac{\rho_{IL} \mathcal{R}_g T}{M_{w-IL}} H$$ (10)

Where $\rho_{IL}(kg.m^{-3})$, $\mathcal{R}_g(J.K^{-1}.mol^{-1})$, $M_{w-IL}$ $(kg.mol^{-1})$, $H(Pa^{-1})$ and $T$ $(K)$ are density of IL, gas constant, molar weight of IL, Henrys law solubility constant for $CO_2$ in [emim] [EtSO₄] and temperature, respectively.

### 3.2.2 Tube side
Transport of $CO_2$ in the tube side is given by the following mass balance equation:

$$\frac{\partial C_{CO_2-T}}{\partial t} + D_{CO_2-T}\left[\frac{\partial^2 C_{CO_2-T}}{\partial r^2} + \frac{1}{r}\frac{\partial C_{CO_2-T}}{\partial r} + \frac{\partial^2 C_{CO_2-T}}{\partial z^2}\right] = U_{z-T}\frac{\partial C_{CO_2-T}}{\partial z}$$ (11)

For steady state mode the equation can be written as below:

$$D_{CO_2-T}\left[\frac{\partial^2 C_{CO_2-T}}{\partial r^2} + \frac{1}{r}\frac{\partial C_{CO_2-T}}{\partial r} + \frac{\partial^2 C_{CO_2-T}}{\partial z^2}\right] = U_{z-T}\frac{\partial C_{CO_2-T}}{\partial z}$$ (12)

Where $D_{CO_2-T}(m^2.s^{-1})$, $C_{CO_2-T}(mol.m^{-3})$ and $U_{z-T}(m.s^{-1})$ denotes the tube side $CO_2$ diffusivity, $CO_2$ concentration and gas velocity, respectively.

The diffusion coefficient in the gas side can be estimated by the following equation [34]:

$$D_{CO_2-g} = \frac{0.01013.T^{1.75}(\frac{1}{M_{w-CO_2}}+\frac{1}{M_{w-N_2}})^{0,5}}{P[(\sum \bar{\upsilon}_{CO_2})^{\frac{1}{3}}+(\sum \bar{\upsilon}_{N_2})^{\frac{1}{3}}]^2}$$ (13)

In the above equation $T(K)$, $P$ $(Pa)$, $M_w$ $(g.mol^{-1})$ and ῡ are temperature, pressure, molar weight and atomic diffusion volumes, respectively. Equation 13 has been used in different studies to predict gas side diffusivity in membrane contactor operations [2,35,36].

Velocity profile in the tube is predicted by Newtonian laminar flow equation:

$$U_{z-T}(r) = 2u_g[1 - (\frac{r}{r_1})^2]$$ (14)

10

Where $u_g$ $(m.s^{-1})$ in the equation represents gas average velocity in the tube.

Boundary conditions are listed in table 4.

### 3.2.3 Membrane phase

The model considers non-wetting, partial wetting and full wetting conditions for which the schematic diagram of membrane thickness is shown in figure 3. Boundary conditions for all three modes are listed in table 4. Whatever wetting mode considered equilibrium between $CO_2$ concentrations in the gas and liquid phase has been assumed, following Henry's law. The difference between all three modes is the location of the gas-liquid interface. For no wetting conditions, the gas-liquid interface is at the pore's exit, on the shell side (r = r$_2$). For fully wetted conditions, the interface is at the pores entrance, on the tube side (r = r$_1$). For partially wetted conditions, the interface is inside the membrane's pores (r = r$_w$) between r$_1$ and r$_2$.
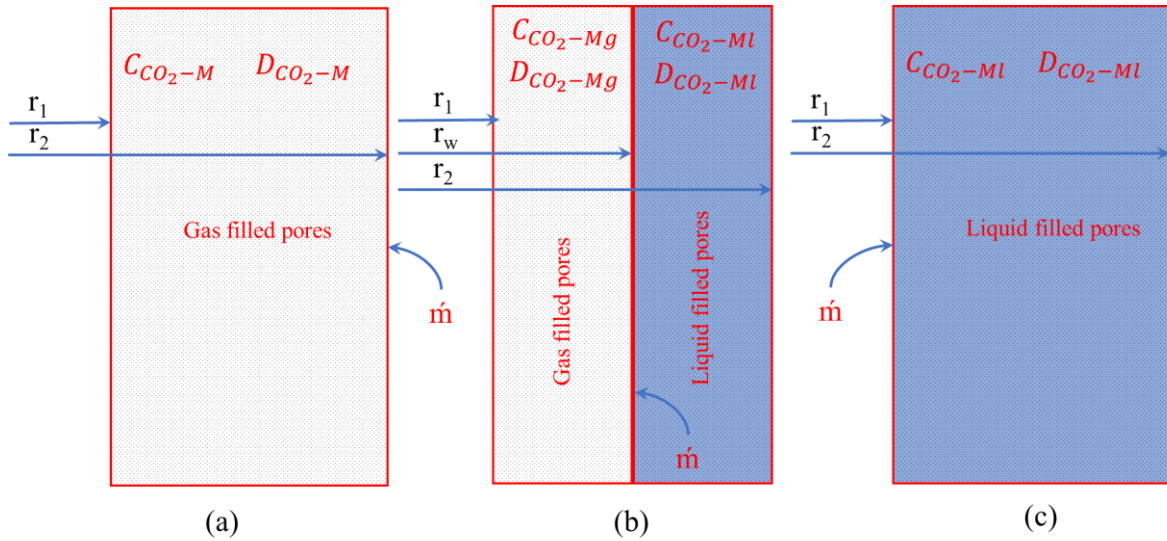
**Figure 3** Schematic diagram of membrane thickness under (a) Non-wetted (b) Partially wetted and (c) Fully wetted conditions

#### 3.2.3.1 No wetting

Mass transport of the $CO_2$ in membrane is only governed by gas diffusion in the pores of membrane. Membrane pores are completely filled with gas. The equation below describes this process:

$$\frac{\partial C_{CO_2-Mg}}{\partial t} + D_{CO_2-Mg}\left[\frac{\partial^2 C_{CO_2-Mg}}{\partial r^2} + \frac{1}{r}\frac{\partial C_{CO_2-Mg}}{\partial r} + \frac{\partial^2 C_{CO_2-Mg}}{\partial z^2}\right] = 0 \tag{15}$$

For steady state:

$$D_{CO_2-Mg}\left[\frac{\partial^2 C_{CO_2-Mg}}{\partial r^2} + \frac{1}{r}\frac{\partial C_{CO_2-Mg}}{\partial r} + \frac{\partial^2 C_{CO_2-Mg}}{\partial z^2}\right] = 0 \tag{16}$$

Where $D_{CO_2-Mg}$ $(m^2.s^{-1})$ and $C_{CO_2-Mg}$ $(mol.m^{-3})$ denotes the $CO_2$ diffusivity and $CO_2$ concentration in membrane, respectively.

A porous membrane is used in this study for which the effective diffusivity is found by the following equation:

11

$$D_{CO_2-Mg} = D_{CO_2-g} \frac{\varepsilon}{\tau} \tag{17}$$

Where $\varepsilon$ and $\tau$ are porosity and tortuosity of the porous membrane.

### 3.2.3.2   Partial wetting

As it's clearly shown in figure 3b, due to IL penetration in the membrane pores, membrane is divided in two sections, gas filled pores and liquid filled pores. Material balance for the transport of $CO_2$ in each section is presented below.

For gas filled portion the only mechanism of $CO_2$ transport is its diffusion in gas (equation 18).

$$\frac{\partial C_{CO_2-Mg}}{\partial t} + D_{CO_2-Mg} \left[ \frac{\partial^2 C_{CO_2-Mg}}{\partial r^2} + \frac{1}{r} \frac{\partial C_{CO_2-Mg}}{\partial r} + \frac{\partial^2 C_{CO_2-Mg}}{\partial z^2} \right] = 0 \tag{18}$$

For steady state:

$$D_{CO_2-Mg} \left[ \frac{\partial^2 C_{CO_2-Mg}}{\partial r^2} + \frac{1}{r} \frac{\partial C_{CO_2-Mg}}{\partial r} + \frac{\partial^2 C_{CO_2-Mg}}{\partial z^2} \right] = 0 \tag{19}$$

For liquid filled portion the only mechanism of $CO_2$ transport is its diffusion in liquid (equation 20):

$$\frac{\partial C_{CO_2-Ml}}{\partial t} + D_{CO_2-Ml} \left[ \frac{\partial^2 C_{CO_2-Ml}}{\partial r^2} + \frac{1}{r} \frac{\partial C_{CO_2-Ml}}{\partial r} + \frac{\partial^2 C_{CO_2-Ml}}{\partial z^2} \right] = 0 \tag{20}$$

For steady state:

$$D_{CO_2-Ml} \left[ \frac{\partial^2 C_{CO_2-Ml}}{\partial r^2} + \frac{1}{r} \frac{\partial C_{CO_2-Ml}}{\partial r} + \frac{\partial^2 C_{CO_2-Ml}}{\partial z^2} \right] = 0 \tag{21}$$

Where $D_{CO_2-Ml}(m^2.s^{-1})$ and $C_{CO_2-Ml}(mol.m^{-3})$ denotes the $CO_2$ diffusivity and $CO_2$ concentration in liquid filled portion of membrane, respectively.

### 3.2.3.3   Full wetting

Just like non-wetting condition in which pores are completely filled with gas, in full wetting the liquid penetrates completely into the membrane pores causing a full wetting condition. Figure 3c shows the membrane thickness filled with liquid penetrating from shell side. The only mechanism of $CO_2$ transport in the membrane is its diffusion in liquid. The transport equation is given below:

$$\frac{\partial C_{CO_2-Ml}}{\partial t} + D_{CO_2-Ml} \left[ \frac{\partial^2 C_{CO_2-Ml}}{\partial r^2} + \frac{1}{r} \frac{\partial C_{CO_2-Ml}}{\partial r} + \frac{\partial^2 C_{CO_2-Ml}}{\partial z^2} \right] = 0 \tag{22}$$

For steady state:

$$D_{CO_2-Ml} \left[ \frac{\partial^2 C_{CO_2-Ml}}{\partial r^2} + \frac{1}{r} \frac{\partial C_{CO_2-Ml}}{\partial r} + \frac{\partial^2 C_{CO_2-Ml}}{\partial z^2} \right] = 0 \tag{23}$$

Where $D_{CO_2-Ml}(m^2.s^{-1})$ and $C_{CO_2-Ml}(mol.m^{-3})$ denotes the $CO_2$ diffusivity and $CO_2$ concentration in liquid filled membrane, respectively.

**Table 4** Boundary conditions for model development under no-wetting, full wetting and partial wetting modes.

| Boundary | Tube Side | Porous Membrane | Shell Side |
|---|---|---|---|
| $z = 0$ | $C_{CO_2-T} = C_0$ | No Flux | Convective Flux |
| $z = L$ | Convective Flux | No Flux | $C_{CO_2-s} = C_{CO_2-Tank}$ (Equation 27) |
| $r = 0$ | $\dfrac{\partial C_{CO_2-T}}{\partial r} = 0$ | - | - |
| $r = r_3$ | - | - | $\dfrac{\partial C_{CO_2-S}}{\partial r} = 0$ |
| **No Wetting** | | | |
| $r = r_1$ | $C_{CO_2-T} = C_{CO_2-Mg}$ | $C_{CO_2-Mg} = C_{CO_2-T}$ | - |
| $r = r_2$ | - | $C_{CO_2-Mg} = \dfrac{C_{CO_2-S}}{ḿ}$ | $C_{CO_2-S} = ḿ\, C_{CO_2-Mg}$ |
| **Full Wetting** | | | |
| $r = r_1$ | $C_{CO_2-T} = \dfrac{C_{CO_2-Ml}}{ḿ}$ | $C_{CO_2-Ml} = ḿ C_{CO_2-T}$ | - |
| $r = r_2$ | - | $C_{CO_2-Ml} = C_{CO_2-S}$ | $C_{CO_2-S} = C_{CO_2-M}$ |

**Partial Wetting**

| Boundary | Tube Side | Gas filled portion | Liquid filled portion | Shell Side |
|---|---|---|---|---|
| $z = 0$ | $C_{CO_2-T} = C_0$ | No Flux | No Flux | Convective Flux |
| $z = L$ | Convective Flux | No Flux | No Flux | $C_{CO_2-s} = C_{CO_2-Tank}$ (Equation 27) |
| $r = 0$ | $\dfrac{\partial C_{CO_2-T}}{\partial r}=0$ | - | - | - |
| $r = r_1$ | $C_{CO_2-T} = C_{CO_2-Mg}$ | $C_{CO_2-Mg} = C_{CO_2-T}$ | - | - |
| $r = r_w$ | - | $C_{CO_2-Mg} = \dfrac{C_{CO_2-Ml}}{ḿ}$ | $C_{CO_2-Ml} = ḿ C_{CO_2-Mg}$ | - |
| $r = r_2$ | - | - | $C_{CO_2-Ml} = C_{CO_2-S}$ | $C_{CO_2-S} = C_{CO_2-Ml}$ |
| $r = r_3$ | - | - | - | $\dfrac{\partial C_{CO_2-S}}{\partial r} = 0$ |

## 3.3 Dynamic model for recycled absorbent

The equations discussed in preceding section describe the steady state transport of $CO_2$ for a single run through the HFMC. The model adopts a setup in which the absorbent is recirculated to a tank, until a pseudo-steady state is achieved for the absorbent in the tank. A differential transient equation has been

developed across the tank to measure the continuous evolution of $CO_2$ in the absorbent. The absorbent passing from the contactor leaves the contactor at time $t$ entering the tank, and exits the tank at $t + \Delta t$ with different concentration.

$$Q_{IL}\left(C_{CO_2-Z=0}(t) - C_{CO_2-tank}(t)\right) = V_{IL}\frac{dC_{CO_2-tank(t)}}{dt} \tag{24}$$

Where $C_{CO_2-tank}(t)$ and $C_{CO_2-Z=0}(t)$ are $CO_2$ concentrations $(mol.m^{-3})$ in tank at time $t$ and shell side concentration $(mol.m^{-3})$ of $CO_2$ at z=0 which is exit of contactor to the absorbent tank, respectively. $V_{IL}$ $(m^3)$ and $Q_{IL}(m^3.s^{-1})$ are total volume and volumetric flow rate of ionic liquid, respectively. Solving the transient equation 24 further for time $t + \Delta t$ gives:

$$Q_{IL}\left(C_{CO_2-Z=0}(t) - C_{CO_2-tank}(t)\right) = V_{IL}\left[\frac{C_{CO_2-Tank}(t+\Delta t)-C_{CO_2-Tank}(t)}{\Delta t}\right] \tag{25}$$

$C_{CO_2-Tank}(t + \Delta t)$ represents $CO_2$ concentrations $(mol.m^{-3})$ in tank at time $t + \Delta t$. Concentration $C_{CO_2-Z=0}(t)$ was found using the following boundary integration equation:

$$C_{CO_2-Z=0}(t) = \frac{\int\int_{r=r_2}^{r=r_3} C_{CO_2-S}(r)rdrd\theta}{\int\int_{r=r_2}^{r=r_3} rdrd\theta} \tag{26}$$

Solving equation 25 for time $t + \Delta t$ gives the following equation:

$$C_{CO_2-Tank}(t + \Delta t) = \frac{\Delta t}{\mathcal{T}_{IL}}C_{CO_2-Z=0}(t) + C_{CO_2-Tank}(t)[1 + \frac{\Delta t}{\mathcal{T}_{IL}}] \tag{27}$$

$\mathcal{T}_{IL}$ is the residence time of ionic liquid in the tank which is found from the following equation:

$$\mathcal{T}_{IL} = \frac{V_{IL}}{Q_{IL}} \tag{28}$$

The concentration in the tank found from Equation (27) is feed to contactor shell side inlet at z=L.

### 3.4    Design basis and model simulation

The above model equations for all domains with appropriate boundary conditions and process parameters were solved using COMSOL Multiphysics® (version 5.3, 2018) which uses finite element method (FEM), and MATLAB R2017a using LiveLink™ for MATLAB. PARDISO solver is used for the steady state model equations. For pseudo-steady state studies a time dependent solver was used to solve non-steady state equations, keeping the same mapping and solver configurations. Geometry is meshed after defining all the parameters and model equations for respective domains. More refined meshes were applied on mass transfer boundaries, especially at interface. Parametric studies were performed by post processing in COMSOL.

Fresh feed gas mixture input at inner side of fibers has a constant concentration of $CO_2$. Absorbent passing through the shell is recirculated from a tank. With each recirculation of absorbent from the tank, the concentration of $CO_2$ increases in the absorbent. The process was started from introducing a fresh absorbent from the tank at shell side of the contactor. After passing through the contactor, absorbent concentration at shell side exit $C_{CO_2-Z=0}(t)$, is predicted by boundary integral equation (26) after first single run in the contactor.  Dynamic equations of absorbent tank developed in section 2.3 coupled with

14

steady state equations of the shell side was able to measure the change in concentration of $CO_2$ in the absorbent tank for the next run through the contactor. Concentration measured by the dynamic equation was feed as input concentration of $CO_2$ in the absorbent at shell side of the contractor (Table 3: BC for shell side at z=L). The coupled process was kept continued until reaching the pseudo-steady state.

## 4 Results and discussion

### 4.1 Experimental results and model validation

Carbon dioxide absorption experiments were carried out at room temperature and nearly ambient pressure conditions. IL was recirculated at a constant flow rate of 60 ml.min^{-1} while gas flow rate was varied from 50 to 100 ml.min^{-1}. IL during recirculation was absorbing $CO_2$ from the gaseous mixture. During the initial recirculation the system was nearly 100 % efficient for both 50 and 100 ml.min^{-1} gas flow rates, based on the removal of $CO_2$ from the gas side. Further recirculation has reduced the efficiency (equation 29), significantly. After 50 minutes of recirculation the efficiency was decreased to 14.1 % and 2.7 % for 50 and 100 ml.min^{-1} gas flow rates, respectively as presented in table 5. Unlike gas side $CO_2$ removal efficiency, $CO_2$ flux and overall mass transfer coefficient increases with increase in gas flow rate for fresh IL in initial recirculation, which have been also reported by Dai and Deng [23]. Initially, $CO_2$ flux was found to be 3.09 $10^{-5}$ mol.m^{-2}.s[-1] and 6.1 $10^{-5}$ mol.m^{-2}.s[-1] for 50 and 100 ml.min^{-1} gas flow rates. The $CO_2$ flux was nearly double for 100 ml.min^{-1} initially, when the IL was fresh having very little amount of $CO_2$. Overall mass transfer coefficient for 100 ml.min^{-1} gas flow rate was 3.99 $10^{-5}$ m.s^{-1} while for 50 ml.min^{-1} gas flow rate it was 3.01 $10^{-5}$ m.s^{-1}. This contrary phenomenon occurs at higher recirculation times after absorbing enough amount of $CO_2$. After 20 minutes, the $CO_2$ flux was reported to be 1.32 $10^{-5}$ mol.m^{-2}.s[-1] for 100 ml.min^{-1} gas flow rate, which is nearly half of the value (2.87 $10^{-5}$ mol.m^{-2}.s[-1]) at 50 ml.min^{-1} gas flow rate, unlike initial times. A greater difference in overall mass transfer coefficient was observed for both gas flow rates at higher recirculation times. After 20 minutes the values noted were 1.21 $10^{-5}$ m.s^{-1} and 0.22 $10^{-5}$ m.s^{-1} for 50 and 100 ml.min^{-1} gas flow rates, respectively.

$$Efficiency\ (\%) = \epsilon = \left(1 - \frac{c_{CO_2-out}}{c_{CO_2-in}}\right) 100 \tag{29}$$

**Table 5** $CO_2$ removal efficiency, gas side flux and overall mass transfer coefficient.

| $Time\ (min)$ | $Q_g (ml.min^{-1})$ | $\epsilon\ (\%)$ | $J_{CO_2} * 10^5 (mol.m^{-2}s^{-1})$ | $K_{exp} * 10^5\ (m.s^{-1})$ |
|---|---|---|---|---|
| Initial | 50 | 99.9 | 3.09 | 3.01 |
|  | 100 | 98.7 | 6.10 | 3.99 |
| 10 | 50 | 98.7 | 3.05 | 1.99 |
|  | 100 | 68.0 | 4.20 | 1.05 |
| 20 | 50 | 92.7 | 2.87 | 1.21 |
|  | 100 | 21.4 | 1.32 | 0.22 |
| 30 | 50 | 38.7 | 1.19 | 0.22 |
|  | 100 | 6.7 | 0.41 | 0.06 |
| 40 | 50 | 23.8 | 0.73 | 0.13 |
|  | 100 | 3.4 | 0.21 | 0.03 |
| 50 | 50 | 14.1 | 0.43 | 0.70 |
|  | 100 | 2.7 | 0.16 | 0.03 |

For the model validation the experimental results of gas side outlet dimensionless concentration of $CO_2$ against recirculation time was plotted and compared with the simulation results. The experimental results were presented with standard error bars. The ionic liquid flow rate and $CO_2$ feed concentration were kept constant at 60 ml.min$^{-1}$ and 15 % by volume, respectively. Surface tension of the IL [emim][EtSO$_4$] is low compared to water, this factor increases the risk of wetting. However, no wetting assumptions were considered for the current process due to the fact that this IL has a very high value of viscosity. Moreover, the process was carried out with hydrophobic membranes having small pore size of 0.04 µm and a slight transmembrane pressure difference was applied (table 2). In order to validate the model, two different sets of operating parameters (50 ml.min$^{-1}$ and 100 ml.min$^{-1}$gas flow rates) were considered. Both parameters have an influence on the separation efficiency.

Figure 4 presents the results obtained for a gas flow rate of 50 ml.min$^{-1}$, whereas figure 5 shows the results for the higher value of the gas flow rate (100 ml.min$^{-1}$). Figure 4 shows a gradual increase in $CO_2$ outlet dimensionless concentration by increasing recirculation time, as the absorbent moves toward saturation with more recirculation and absorption. If we consider the experimental errors represented as bars on the figure there was a quite good agreement between experimental and simulation results.
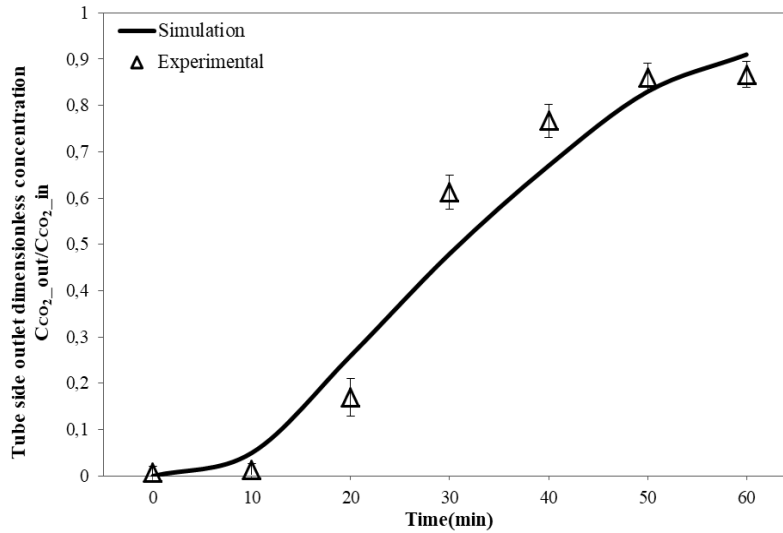


**Figure 4** Comparison of current simulation with experimental data for $CO_2$ absorption at recirculation time under non-wetting assumption; $Q_{IL} = 60 \ ml.min^{-1}$, $Q_g = 50 \ ml.min^{-1}$, $\varphi_v = 15 \ \%$.

Figure 5 shows similar results. A rather good agreement between experimental and simulation results was also observed, especially at higher recirculation times. The assumption of non-wetted membrane seems validated in regards with the agreement between modeled and experimental results. As can be seen later in section 3.3, if the membrane were partially wetted, the efficiency would decrease and the gas side $CO_2$ concentration ratio ($C_{CO2\_out}/C_{CO2\_in}$) would be higher. Nevertheless, we can conclude that the model matches well the experimental results. Moreover, considering the experimental errors, the standard deviation between the calculated and experimental results is ranged only between 3% to 5%.

The dynamic mode was adopted to validate the model for the developed experimental setup. Further results developed using the same model are for first single run through the contactor, with fresh absorbent and in non-recirculation mode. Once the model is validated, it could be further used to study the effect of other parameters.
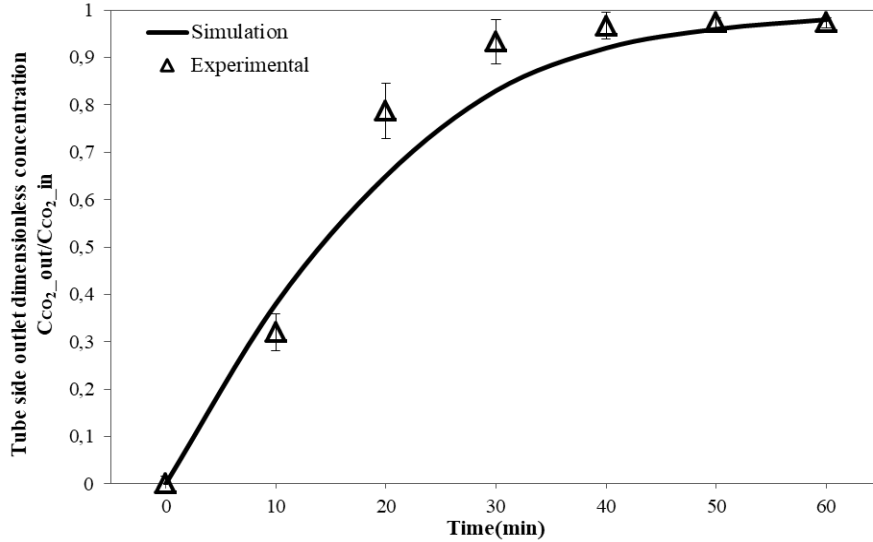


**Figure 5** Comparison of current simulation with experimental data for $CO_2$ absorption at recirculation time under non-wetting assumption; $Q_{IL} = 60 \ ml.min^{-1}$, $Q_g = 100 \ ml.min^{-1}$, $\varphi_v = \ 15 \ \%$.

## 4.2 Concentration distribution of $CO_2$ under non-wetting mode

Figure 6 shows concentration distribution of $CO_2$ in tube, membrane and shell of the contactor under no-wetting mode. The gas mixture flows in the inner (tube) side from z=0, where its concentration is maximum ($C_0$), towards z=L. Absorbent is allowed to flow counter currently in the shell side, as it enters at z=L where $CO_2$ concentration is minimum and moves towards z=0 while absorbing $CO_2$ which diffuses from the walls of porous membrane. Concentration difference (driving force) causes to diffuse $CO_2$ through the walls of porous membrane from tube side towards shell side. Diffusion is the dominant mass transfer mechanism in radial direction due to the huge concentration difference while in axial direction convection is the dominant mechanism due to fluid flow. Figure 6 shows that $CO_2$ concentration decreases gradually as it moves forward in the contactor while it increases in the shell side when the absorbent moves forward in the shell of the contactor.

17
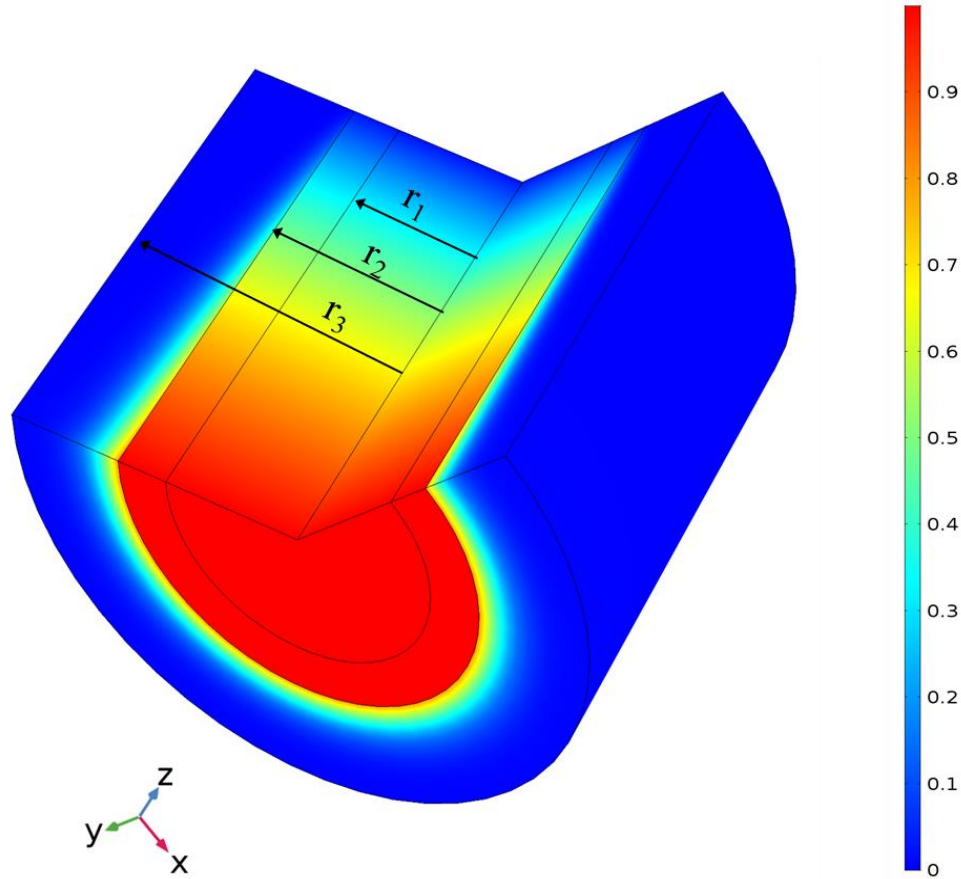
**Figure 6** Overall dimensionless concentration profile of $CO_2$ (tube, membrane and shell) under non-wetting assumption; steady state, $Q_{IL} = 50\ ml.min^{-1}$, $Q_g = 20\ ml.min^{-1}$, $\varphi_v = 15\ \%$, $T = 291K$.

### 4.3 Effect of membrane wetting on $CO_2$ removal

Wetting is a major challenge in membrane contactor operations as it significantly increases the mass transfer resistance. Some studies predict that wetting can cause six times drop in $CO_2$ absorption and that 5 % wetting can cause up to 20% reduction in mass transfer coefficient [4,37,38]. Therefore, five different membrane wetting conditions have been investigated. Apart from non-wetted and fully wetted conditions, three partially wetted conditions have been considered: 5% wetting, 20% wetting and 50% wetting. X% wetting means that X% of the pore's length is filled with ionic liquid.

Figure 7 presents the drop in $CO_2$ absorption efficiency with increase in membrane wetting. A significant reduction in mass transfer can be seen due to membrane wetting. A 5% membrane wetting has caused almost 40 % reductions in the separation efficiency. A major drop in efficiency can be observed by wetting of a small portion of membrane. Efficiency of $CO_2$ separation drops from 97% to 20 % when conditions changes from non-wetting to full wetting mode.

Where $\frac{c_{CO_2-out}}{c_{CO_2-in}}$ represents tube side outlet dimensionless concentration of $CO_2$.

18
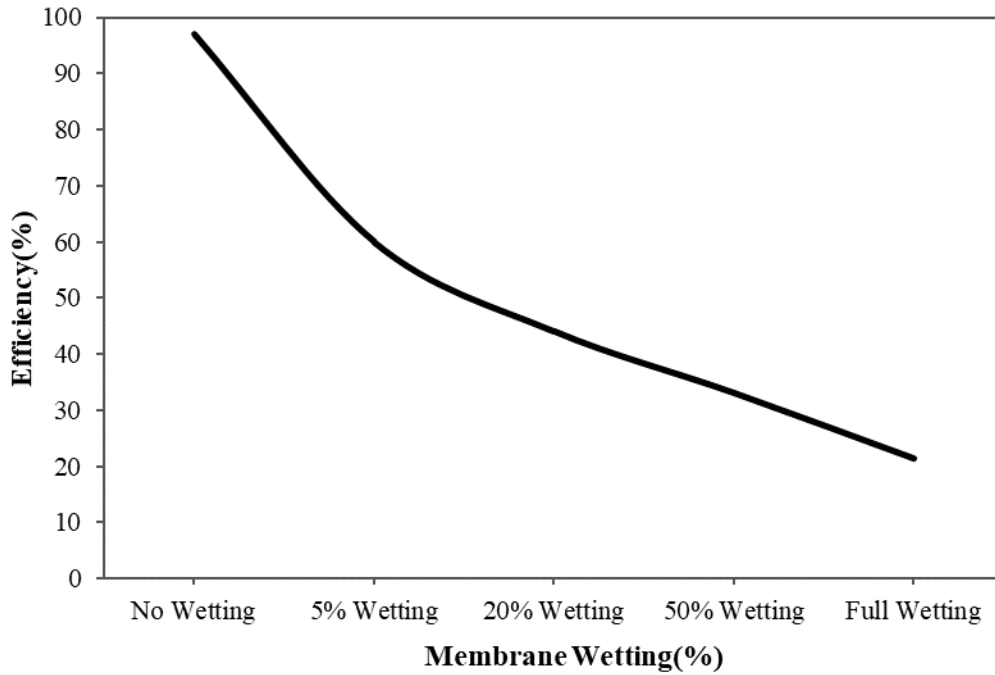
**Figure 7** Effect of membrane wetting on separation efficiency of $CO_2$; steady state, $Q_{IL} = 50\ ml.\ min^{-1}$, $Q_g = 20\ ml.\ min^{-1}$, $\varphi_v = 15\ \%$, $T = 291K$.

Figure 8 presents concentration distribution of $CO_2$ in membrane under partial wetting and full wetting mode. Figure 8 (a), (b) and (c) represents membranes under 5%, 20% and half wetting conditions, respectively, while figure 8(d) represents full wetting mode. It can be observed that increase in membrane wetting causes a significant increase in $CO_2$ dimensionless concentration at outlet of contactor and reduces efficiency of separation. In partial wetting modes, a completely different concentration distribution can be observed in wetted and non-wetted portion of membrane due to the increase of the mass transfer resistance in the wetted portion.
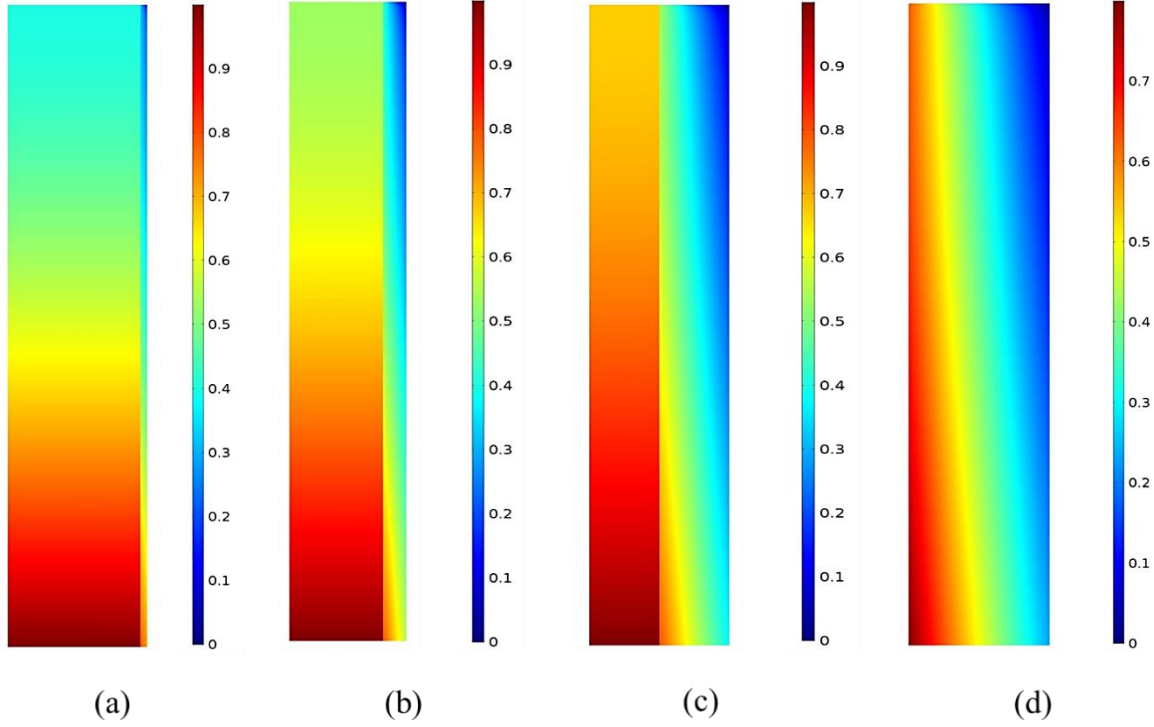
**Figure 8** Dimensionless concentration distribution of $CO_2$ along porous membrane (a) 5% wetting (b) 20% wetting (c) half wetting (d) full wetting; steady state, $Q_{IL} = 50\ ml.min^{-1}$, $Q_g = 20\ ml.min^{-1}$, $\varphi_v = 15\ \%$, $T = 291K$.

The fully wetted membrane presents a very low separation efficiency therefore this condition will not be further taken into account and focus will be put on non-wetted and partially wetted conditions.

### 4.4 Effect of membrane porosity and tortuosity

It is clear from equation (17) that porosity has a significant effect on the mass transfer of $CO_2$. A higher porosity will reduce membrane mass transfer resistance and process will be much efficient [39]. In this study, the effect of membrane porosity on $CO_2$ removal efficiency was investigated and reported in figure 9. Porosity has also direct effect on tortuosity of the membrane. An increase in porosity decreases tortuosity which makes the process more efficient. Tortuosity was varied according to the following equation [40]:

$$\tau = \frac{1}{\varepsilon} \tag{30}$$

In non-wetting conditions increasing porosity from 0.1 to 0.5 increased efficiency by 53 %. In case of 20 % wetting an increase of 42 % was observed. From above results it can be clearly concluded that lower porosity has increased membrane mass transfer resistance. However, in terms of membrane manufacturing, there are some limitations on membrane porosity enhancement due to fabrication and mechanical strength problems.
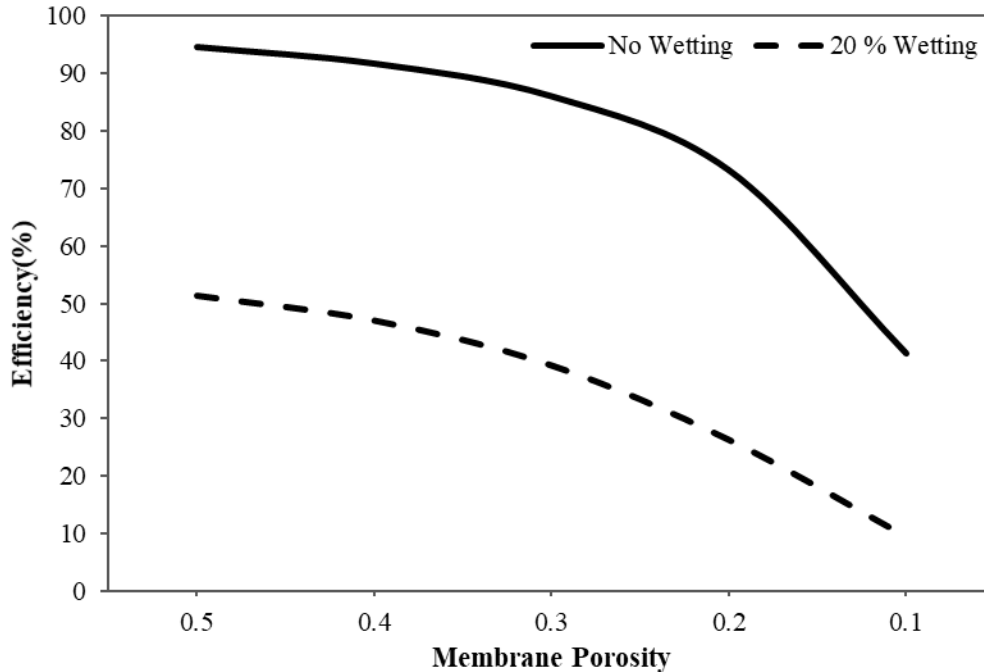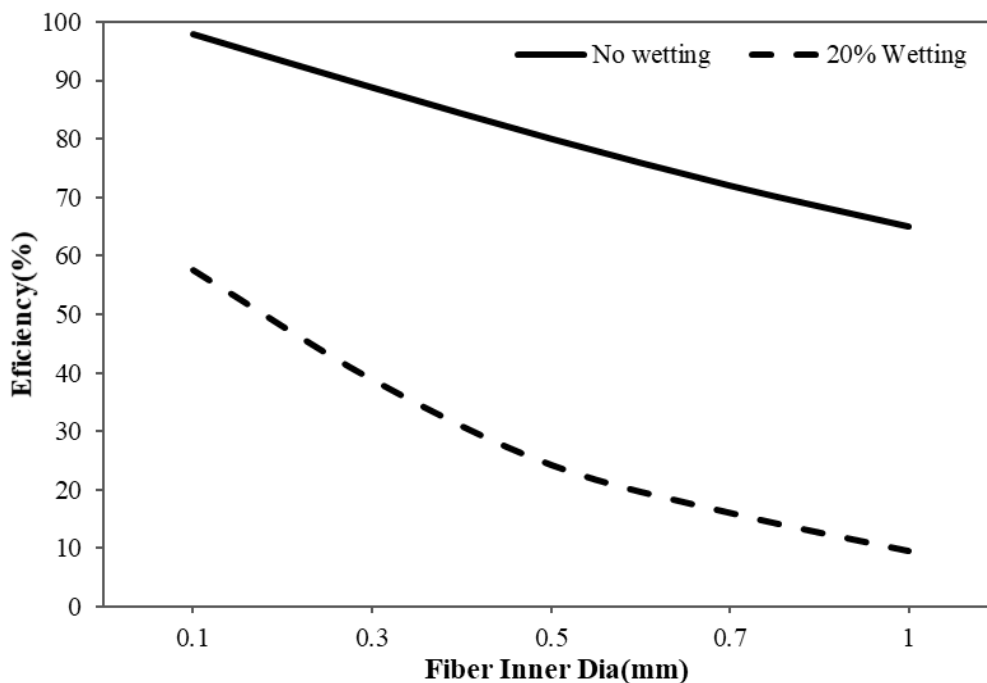
**Figure 9** Effect of membrane porosity on separation efficiency of CO2 under non-wetted and partially wetted modes; steady state, $Q_{IL} = 50\ ml.\,min^{-1}$, $Q_g = 20\ ml.\,min^{-1}$, $\varphi_v = 15\ \%$, $T = 291K$,

Tortuosity can directly affect the mass transfer resistance in porous membrane. Increase in tortuosity increases the mass transfer resistance in porous membrane [39]. Keeping a constant value of porosity (0.5), an increase in tortuosity significantly affected the removal efficiency. A decrease of about 20 % in removal efficiency was observed by changing tortuosity value from 1 to 7 in non-wetting mode. In case of 20 % wetting, the removal efficiency decreased by 22 %.

## 4.5　Effect of fiber diameter and module length

In the current study gas is allowed to flow inside the fiber. Increasing fiber inner diameter will increase gas volume. Number of fibers, gas and liquid velocities and other dimensions were kept constant. Increase in fiber inner diameter which in turn causes an increase in gas volume makes the process less efficient. As other dimensions and conditions were kept constant, there was more $CO_2$ available for the same amount of absorbent, which reduced separation efficiency. A smaller inner diameter will enhance the separation efficiency as shown in figure 11. The effect of changing fiber diameter has been studied and confirmed by Dai et al. [2]. Fiber inner diameter was changed from 5 mm to 1mm which effectively enhanced separation efficiency. Ahmad et al.[6] and Zhang et al[21] reported opposite effects when absorbent was passed inside the fiber. Increasing the fiber diameter has enhanced $CO_2$ separation due to increase in mass transfer area.

A significant drop in removal efficiency was observed by increasing fiber inner diameter, for both non-wetted and partially wetted modes. In no wetting conditions changing fiber inner diameter from 0.1 mm to 1 mm reduced efficiency by 33%. In case of 20 % wetting the efficiency is reduced by 47%.

**Figure 10** Effect of fiber inner diameter on separation efficiency of $CO_2$ under non-wetted and partially wetted modes; steady state, $Q_{IL} = 50 \; ml.min^{-1}$, $Q_g = 20 \; ml.min^{-1}$, $\varphi_v = 15 \%$, $T = 291K$.

Increase in membrane length causes an increase in mass transfer surface area and increase in absorbent residence time in module, which enhances the process efficiency. A significant increase in efficiency was observed with increase in module length, for both non-wetted and partially wetted conditions, during the simulations. Similar effects have been confirmed in other studies. Ahmad et al. [41] reported that increasing module length enhances separation performance, while separating carbon dioxide from methane in HFMCs. Increasing fiber length will increase permeation which in turn will enhance absorption performance. In another study by Zhang et al. [42], the fiber length was increased from 200 cm to 1000 cm which increased the $CO_2$ absorption efficiency in piperazine from 56% to 84 %. Wang et al. [43] also reported the same effects in membrane stripping for $CO_2$ desorption from MEA. It was reported that long residence time in membrane contactor due to increased membrane length has resulted in better separation performances. An initial change in module length causes more variation in removal efficiency. The variation in removal efficiency decreases with further change in module length

In this study, pressure drop in the membrane module is not considered. Increase in length may cause a higher pressure drop due to high absorbent viscosity which in turn may cause membrane wetting. $CO_2$ concentration also drops progressively along membrane length which reduces driving force for separation [2]. Thus, an optimized value for membrane module length must be used for optimum separations.

### 4.6    Effect of gas and absorbent flow rate

Effect of gas flow rate on $CO_2$ removal efficiency is shown in figure 11. A smaller gas flow rate provides better removal efficiency. Increasing gas flow rate leads to minimal gas residence time in the tube, which leads to allow more $CO_2$ to pass from the contactor without absorption. This decrease in $CO_2$ residence time considerably decreases its removal efficiency[44,45]. Although $CO_2$ absorption efficiency decreases

with increase in gas flow rate, the amount of $CO_2$ absorbed in the liquid phase will increase. The $CO_2$ absorption efficiency decreases as there is more $CO_2$ available at gas outlet which is not absorbed due to high gas flow rate. However, the $CO_2$ amount in the liquid phase increases because of the enhanced mass transfer[46]. This enhancement in mass transfer is due to the greater average concentration of $CO_2$ at gas side because of the higher gas flow rate[47].

Figure 11 shows dimensionless concentration of $CO_2$ against radial dimensionless length at outlet of the tube. It is evident from figure that increasing gas flow rate has significantly decreased the removal efficiency, for both non-wetted and partially wetted modes. Gas flow rate was varied from 10 ml.min^{-1} to 130 ml.min^{-1} while keeping a constant absorbent flow rate at 50 ml.min^{-1}. $CO_2$ dimensionless concentration at the outlet of the tube was increased by 35 % and 38 % in non-wetting and partial wetting modes, respectively, by varying gas flow rate from 10 ml.min^{-1} to 130 ml.min^{-1}. Gas flow rate should be very carefully optimized as it directly affects the $CO_2$ transport and also causes a high/low $CO_2$ flux across membrane.
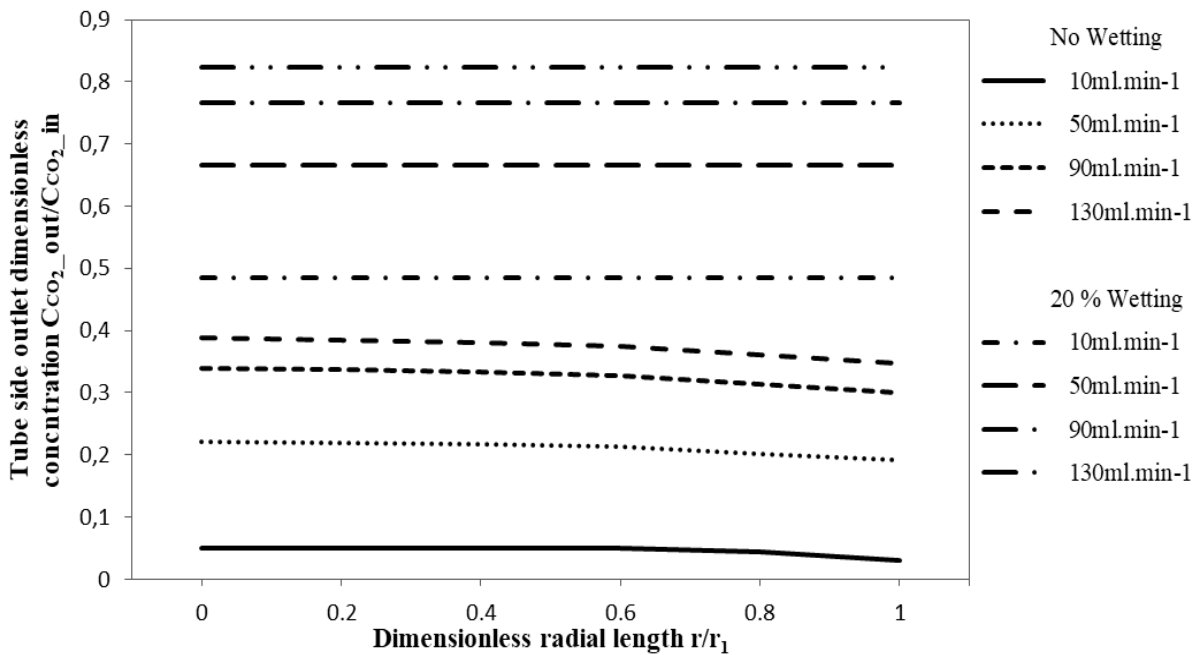


**Figure 11** Effect of gas flow rate on separation performance of $CO_2$ under non-wetted and partially wetted modes; steady state, $Q_{IL} = 50 \, ml. min^{-1}$, $\varphi_v = 15 \%$, $T = 291K$.

Absorbent flow rate can affect the $CO_2$ removal efficiency, as shown in figure 12. An increase in absorbent flow rate increases removal efficiency [45]. A lower absorbent flow rate reduces the driving force for the $CO_2$ due to the lower concentration difference. Increasing absorbent flow rate allows more fresh absorbent to enter the system and absorb $CO_2$. It also increases the volume of absorbent for the same amount of $CO_2$ in gas phase. Increasing absorbent flow rate also reduces liquid boundary layer thickness which results in an increase in liquid mass transfer coefficient and diffusivity [45,46,48,49]. $CO_2$ flux was increased by increasing water and NaOH flow rate in PVDF membrane contactor. Wang at al. [50]

reported that increasing absorbent flow rate increases the $CO_2$ absorption flux because of the instantaneous absorption.

Absorbent flow rate was varied from 5 ml.min$^{-1}$ to 65 ml.min$^{-1}$ while gas flow rate was kept constant at 130 ml.min$^{-1}$. A higher gas flow rate was used to study the effect of absorbent flow rate on process efficiency. At lower gas flow rates, the process was efficient enough which made it impossible to study the effect of higher absorbent flow rates. $CO_2$ dimensionless concentration at the outlet of the tube dropped by 12% and 16% for non-wetting and partial wetting modes, respectively, by increasing liquid flow rate from 5 ml.min$^{-1}$ to 65 ml.min$^{-1}$.

Apart from the enhancement in the $CO_2$ removal efficiency with increase in absorbent flowrate, several authors have reported the influence of absorbent flowrate on the membrane wetting [37]. A significant increase in pore wetting due to increase in absorbent flowrate has been reported. Boributh et al. [51] while increasing the absorbent velocity from 0.1 m s$^{-1}$ to 0.4 m s$^{-1}$ observed an increase in the wetting ratio by a factor of approximately 8. One of the studies has attributed this increase in wetting as to be due to the reduction in absorbent boundary resistance with increase in absorbent flowrate which has increased the resistance due to the absorbent inside the pores of membrane (wetted part of the membrane) [52]. Mavroudi et al. [53] while working on the $CO_2$ absorption in water-membrane contactor setup observed that total mass transfer resistance increases with time and becomes more significant at higher absorbent flowrates. These authors have reported that this behavior might be due to the possible increase in pressure with increase in absorbent flowrate, thus resulting higher transmembrane pressure and increasing membrane pore wetting. An optimized value of absorbent flow rate is required to reduce the potential for wetting and to control both capital and operational cost for the process [45,54].
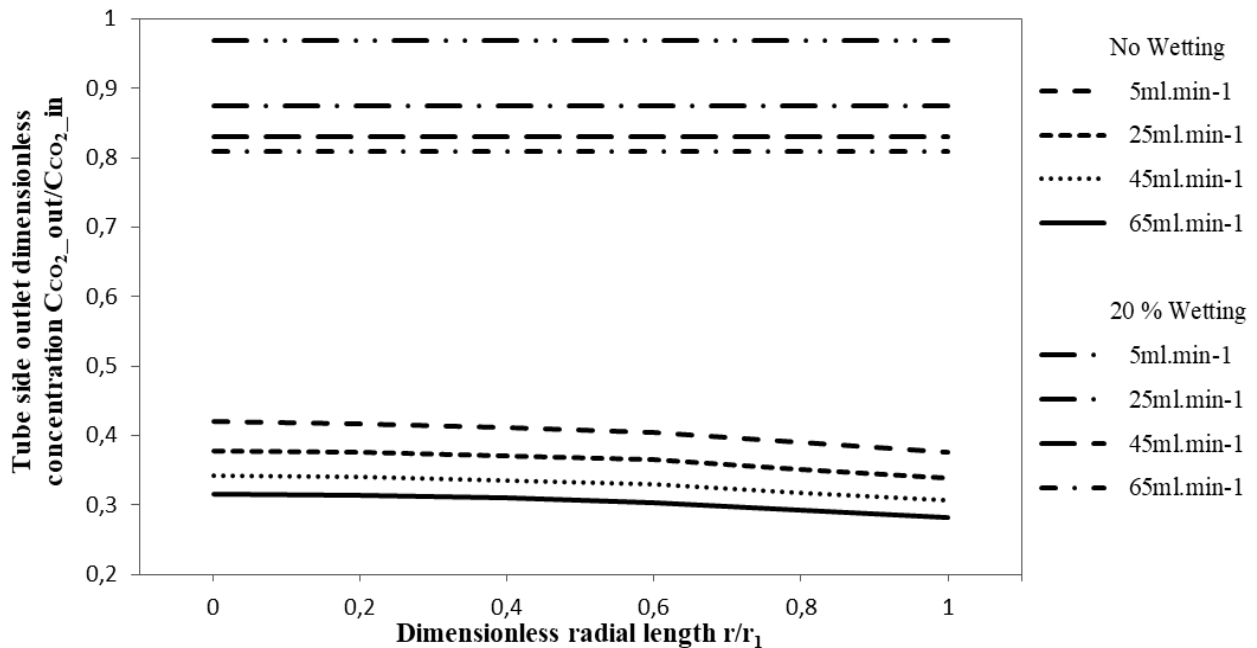


**Figure 12** Effect of absorbent flow rate on separation performance of $CO_2$ under non-wetted and partially wetted modes; steady state, $Q_g = 130 \, ml.min^{-1}$, $\varphi_v = 15\,\%$, $T = 291K$.

It can be observed that there is a minor drop in concentration when we move toward the wall of the membrane ($r_1$), in no-wetting mode. It may be due to the absorption and driving force toward membrane which reduces its concentration near the membrane wall. On the other hand, in partial wetting condition there is almost no drop in concentration which may be due to the reduction in driving force due to wetting and increased membrane mass transfer resistance.

## 5    Conclusions

The present work aims to study the absorption process of $CO_2$ from $CO_2/N_2$ mixture in HFMC coupled with 1-Ethyl-3-methylimidazolium ethylsulfate [emim][EtSO$_4$] as an absorbent. A dynamic 2D mass-transfer model was developed considering non-wetted, partially wetted and fully wetted conditions for a counter current flow in contactor. $CO_2$ flux, removal efficiency and overall mass transfer coefficients were investigated against time for pseudo-steady state absorption. Effect of membrane wetting on $CO_2$ absorption process was systematically studied. Effects of porosity, module length, fiber inner diameter, gas flow rate and absorbent flow rate on $CO_2$ absorption efficiency were studied considering both non-wetted and partially wetted conditions. Some of the findings are listed below.

- IL upon recirculation absorbs $CO_2$ until reaching pseudo-steady state. For fresh IL (or very low concentration of $CO_2$), at higher gas flowrates the $CO_2$ flux and overall mass transfer coefficient are much higher compared to that at low gas flowrates. This effect becomes opposite at higher recirculation times after absorption of $CO_2$ in IL.
- Membrane wetting has a significant effect on $CO_2$ absorption process. Only a 5% wetting can cause a drop of 40% in $CO_2$ removal efficiency.
- Increasing membrane porosity increases the $CO_2$ removal efficiency for both wetted and non-wetted membranes. Membrane tortuosity has the opposite effect on removal efficiency. $CO_2$ removal efficiency is favored by increase in module length and a decrease in fiber inner diameter.
- A decrease in gas flowrate and increase in absorbent flow rate favors $CO_2$ removal efficiency.

Even if ILs are for the instance relatively expensive and then difficult to be applied at industrial scale, their stability, lack of reactivity towards the membrane material, reusability and low vapor pressure made them good solvent models for this process. Moreover, in addition to the main drawback of high cost they have a relatively high viscosity. Indeed, current experimental research is being carried out using mixtures of various ILs with water in order to decrease their viscosity and process costs. Also, an experimental and modeling work on stripping or desorption process is under way.

## References

[1]    Z. Dai, R.D. Noble, D.L. Gin, X. Zhang, L. Deng, Combination of ionic liquids with membrane technology: A new approach for CO2separation, J. Memb. Sci. 497 (2016) 1–20. doi:10.1016/j.memsci.2015.08.060.

[2]    Z. Dai, M. Usman, M. Hillestad, L. Deng, Modelling of a tubular membrane contactor for pre-combustion CO 2 capture using ionic liquids: Influence of the membrane configuration, absorbent properties and operation parameters, Green Energy Environ. 1 (2016) 266–275. doi:10.1016/j.gee.2016.11.006.

[3]    E. Chabanon, D. Roizard, E. Favre, Modeling strategies of membrane contactors for post-combustion carbon capture: A critical comparative study, Chem. Eng. Sci. 87 (2013) 393–407. doi:10.1016/j.ces.2012.09.011.

[4]    S. Zhao, P.H.M. Feron, L. Deng, E. Favre, E. Chabanon, S. Yan, J. Hou, V. Chen, H. Qi, Status and progress

of membrane contactors in post-combustion carbon capture: A state-of-the-art review of new developments, J. Memb. Sci. 511 (2016) 180–206. doi:10.1016/j.memsci.2016.03.051.

[5]     R. Fazaeli, S.M.R. Razavi, M. Sattari Najafabadi, R. Torkaman, A. Hemmati, Computational simulation of $CO_2$ removal from gas mixtures by chemical absorbents in porous membranes, RSC Adv. 5 (2015) 36787–36797. doi:10.1039/C5RA02001H.

[6]     A. Azari, M. Ali, H. Sanaeepur, International Journal of Greenhouse Gas Control CFD study of CO 2 separation in an HFMC : Under non-wetted and partially-wetted conditions, 49 (2016) 81–93.

[7]     A. Muhammad, M. Younas, M. Rezakazemi, Quasi-dynamic modeling of dispersion-free extraction of aroma compounds using hollow fiber membrane contactor, Chem. Eng. Res. Des. 127 (2017) 52–61. doi:10.1016/j.cherd.2017.09.007.

[8]     A. Gabelman, S.-T. Hwang, Hollow fiber membrane contactors, J. Memb. Sci. 159 (1999) 61–106. doi:10.1016/S0376-7388(99)00040-X.

[9]     M. Pourafshari Chenar, M. Soltanieh, T. Matsuura, A. Tabe-Mohammadi, K.C. Khulbe, The effect of water vapor on the performance of commercial polyphenylene oxide and Cardo-type polyimide hollow fiber membranes in CO2/CH4 separation applications, J. Memb. Sci. 285 (2006) 265–271. doi:10.1016/j.memsci.2006.08.028.

[10]    K. Villeneuve, A.A. Torres Hernandez, D. Albarracin Zaidiza, D. Roizard, S. Rode, Effects of water condensation on hollow fiber membrane contactor performance for CO2capture by absorption into a chemical solvent, J. Memb. Sci. 556 (2018) 365–373. doi:10.1016/j.memsci.2018.04.005.

[11]    I. Sreedhar, T. Nahar, A. Venugopal, B. Srinivas, Carbon capture by absorption – Path covered and ahead, Renew. Sustain. Energy Rev. 76 (2017) 1080–1107. doi:10.1016/j.rser.2017.03.109.

[12]    M. Hasib-ur-Rahman, M. Siaj, F. Larachi, Ionic liquids for CO2capture-Development and progress, Chem. Eng. Process. Process Intensif. 49 (2010) 313–322. doi:10.1016/j.cep.2010.03.008.

[13]    M. Ramdin, T.W. De Loos, T.J.H. Vlugt, State-of-the-art of CO2 capture with ionic liquids, Ind. Eng. Chem. Res. 51 (2012) 8149–8177. doi:10.1021/ie3003705.

[14]    J. Chau, G. Obuskovic, X. Jie, K.K. Sirkar, Pressure swing membrane absorption process for shifted syngas separation: Modeling vs. experiments for pure ionic liquid, J. Memb. Sci. 453 (2014) 61–70. doi:10.1016/j.memsci.2013.10.038.

[15]    S. Zhang, J. Sun, X. Zhang, J. Xin, Q. Miao, J. Wang, Ionic liquid-based green processes for energy production, Chem. Soc. Rev. 43 (2014) 7838–7869. doi:10.1039/C3CS60409H.

[16]    M.A. Malik, M.A. Hashim, F. Nabi, Ionic liquids in supported liquid membrane technology, Chem. Eng. J. 171 (2011) 242–254. doi:10.1016/j.cej.2011.03.041.

[17]    X. Zhang, X. Zhang, H. Dong, Z. Zhao, S. Zhang, Y. Huang, Carbon capture with ionic liquids: overview and progress, Energy Environ. Sci. 5 (2012) 6668. doi:10.1039/c2ee21152a.

[18]    J. Zhang, S. Zhang, K. Dong, Y. Zhang, Y. Shen, X. Lv, Supported absorption of CO2 by tetrabutylphosphonium amino acid ionic liquids, Chem. - A Eur. J. 12 (2006) 4021–4026. doi:10.1002/chem.200501015.

[19]    L. Gomez-Coma, A. Garea, A. Irabien, Carbon dioxide capture by [emim][Ac] ionic liquid in a polysulfone hollow fiber membrane contactor, Int. J. Greenh. Gas Control. 52 (2016) 401–409. doi:10.1016/j.ijggc.2016.07.019.

[20]    L. Gómez-Coma, A. Garea, Á. Irabien, Hybrid Solvent ([emim][Ac]+water) to Improve the CO2Capture Efficiency in a PVDF Hollow Fiber Contactor, ACS Sustain. Chem. Eng. 5 (2017) 734–743.

doi:10.1021/acssuschemeng.6b02074.

[21]    J.G. Lu, C.T. Lu, Y. Chen, L. Gao, X. Zhao, H. Zhang, Z.W. Xu, CO2capture by membrane absorption coupling process: Application of ionic liquids, Appl. Energy. 115 (2014) 573–581. doi:10.1016/j.apenergy.2013.10.045.

[22]    Z. Dai, L. Ansaloni, L. Deng, Precombustion $CO_2$ Capture in Polymeric Hollow Fiber Membrane Contactors Using Ionic Liquids: Porous Membrane versus Nonporous Composite Membrane, Ind. Eng. Chem. Res. 55 (2016) 5983–5992. doi:10.1021/acs.iecr.6b01247.

[23]    Z. Dai, L. Deng, Membrane absorption using ionic liquid for pre-combustion CO2 capture at elevated pressure and temperature, Int. J. Greenh. Gas Control. 54 (2016) 59–69. doi:10.1016/j.ijggc.2016.09.001.

[24]    J. Happel, Viscous flow relative to arrays of cylinders, AIChE J. 5 (1959) 174–177. doi:10.1002/aic.690050211.

[25]    H. Schmidt, M. Stephan, J. Safarov, I. Kul, J. Nocke, I.M. Abdulagatov, E. Hassel, Experimental study of the density and viscosity of 1-ethyl-3- methylimidazolium ethyl sulfate, J. Chem. Thermodyn. 47 (2012) 68–75. doi:10.1016/j.jct.2011.09.027.

[26]    A.P. Fröba, H. Kremer, A. Leipertz, Density, Refractive Index, Interfacial Tension, and Viscosity of Ionic Liquids [EMIM][EtSO $_4$ ], [EMIM][NTf $_2$ ], [EMIM][N(CN) $_2$ ], and [OMA][NTf $_2$ ] in Dependence on Temperature at Atmospheric Pressure, J. Phys. Chem. B. 112 (2008) 12420–12430. doi:10.1021/jp804319a.

[27]    A.N. Soriano, B.T. Doma, M.H. Li, Carbon dioxide solubility in some ionic liquids at moderate pressures, J. Taiwan Inst. Chem. Eng. 40 (2009) 387–393. doi:10.1016/j.jtice.2008.12.002.

[28]    R.B. Bird, W.E. Stewart, E.N. Lightfoot, Transport Phenomena, 2002. doi:10.1016/j.ijhydene.2006.08.059.

[29]    D. Morgan, L. Ferguson, P. Scovazzo, Diffusivities of gases in room-temperature ionic Liquids: Data and correlations obtained using a lag-time technique, Ind. Eng. Chem. Res. 44 (2005) 4815–4823. doi:10.1021/ie048825v.

[30]    L.F. Zubeir, G.E. Romanos, W.M.A. Weggemans, B. Iliev, T.J.S. Schubert, M.C. Kroon, Solubility and Diffusivity of CO2 in the Ionic Liquid 1-Butyl-3-methylimidazolium Tricyanomethanide within a Large Pressure Range (0.01 MPa to 10 MPa), J. Chem. Eng. Data. 60 (2015) 1544–1562. doi:10.1021/je500765m.

[31]    S.S. Moganty, R.E. Baltus, Diffusivity of Carbon Dioxide in Room-Temperature Ionic Liquids, Ind. Eng. Chem. Res. 49 (2010) 9370–9376. doi:10.1021/ie101260j.

[32]    A.H. Jalili, A. Mehdizadeh, M. Shokouhi, A.N. Ahmadi, M. Hosseini-Jenab, F. Fateminassab, Solubility and diffusion of CO2and H2S in the ionic liquid 1-ethyl-3-methylimidazolium ethylsulfate, J. Chem. Thermodyn. 42 (2010) 1298–1303. doi:10.1016/j.jct.2010.05.008.

[33]    R. Sander, Compilation of Henry's law constants (version 4.0) for water as solvent, Atmos. Chem. Phys. 15 (2015) 4399–4981. doi:10.5194/acp-15-4399-2015.

[34]    E.N. Fuller, P.D. Schettler, J.C. Giddings, A new method for prediction of binary gas-phase diffusion coefficients, Ind. Eng. Chem. 58 (1966) 18–27. doi:10.1021/ie50677a007.

[35]    M. Saidi, Mathematical modeling of CO2absorption into novel reactive DEAB solution in hollow fiber membrane contactors; kinetic and mass transfer investigation, J. Memb. Sci. 524 (2017) 186–196. doi:10.1016/j.memsci.2016.11.028.

[36]    J. Albo, P. Luis, A. Irabien, Absorption of coal combustion fl ue gases in ionic liquids using different membrane contactors, Desalin. Water Treat. 27 (2011) 54–49. doi:10.5004/dwt.2011.2050.

[37]    S. Mosadegh-Sedghi, D. Rodrigue, J. Brisson, M.C. Iliuta, Wetting phenomenon in membrane contactors -

Causes and prevention, J. Memb. Sci. 452 (2014) 332–353. doi:10.1016/j.memsci.2013.09.055.

[38]   R. Wang, H.Y. Zhang, P.H.M. Feron, D.T. Liang, Influence of membrane wetting on CO2 capture in microporous hollow fiber membrane contactors, Sep. Purif. Technol. 46 (2005) 33–40. doi:10.1016/j.seppur.2005.04.007.

[39]   F. Asfand, M. Bourouis, A review of membrane contactors applied in absorption refrigeration systems, Renew. Sustain. Energy Rev. 45 (2015) 173–191. doi:10.1016/j.rser.2015.01.054.

[40]   S.B. Iversen, V.K. Bhatia, K. Dam-Johansen, G. Jonsson, Characterization of microporous membranes for use in membrane contactors, J. Memb. Sci. 130 (1997) 205–217. doi:10.1016/S0376-7388(97)00026-4.

[41]   F. Ahmad, K.K. Lau, S.S.M. Lock, S. Rafiq, A.U. Khan, M. Lee, Hollow fiber membrane model for gas separation: Process simulation, experimental validation and module characteristics study, J. Ind. Eng. Chem. 21 (2015) 1246–1257. doi:10.1016/j.jiec.2014.05.041.

[42]   Z. Zhang, F. Chen, M. Rezakazemi, Chemical Engineering Research and Design Modeling of a CO 2 - piperazine-membrane, 1 (2017) 375–384.

[43]   Z. Wang, M. Fang, H. Yu, Q. Ma, Z. Luo, Modeling of CO $_2$ Stripping in a Hollow Fiber Membrane Contactor for CO $_2$ Capture, Energy & Fuels. 27 (2013) 6887–6898. doi:10.1021/ef401488c.

[44]   S.H. Yeon, K.S. Lee, B. Sea, Y.I. Park, K.H. Lee, Application of pilot-scale membrane contactor hybrid system for removal of carbon dioxide from flue gas, J. Memb. Sci. 257 (2005) 156–160. doi:10.1016/j.memsci.2004.08.037.

[45]   S. ping Yan, M.X. Fang, W.F. Zhang, S.Y. Wang, Z.K. Xu, Z.Y. Luo, K.F. Cen, Experimental study on the separation of CO2from flue gas using hollow fiber membrane contactors without wetting, Fuel Process. Technol. 88 (2007) 501–511. doi:10.1016/j.fuproc.2006.12.007.

[46]   J.L. Li, B.H. Chen, Review of CO2absorption using chemical solvents in hollow fiber membrane contactors, Sep. Purif. Technol. 41 (2005) 109–122. doi:10.1016/j.seppur.2004.09.008.

[47]   H.Y. Zhang, R. Wang, D.T. Liang, J.H. Tay, Modeling and experimental study of CO2absorption in a hollow fiber membrane contactor, J. Memb. Sci. 279 (2006) 301–310. doi:10.1016/j.memsci.2005.12.017.

[48]   A. Mansourizadeh, A.F. Ismail, T. Matsuura, Effect of operating conditions on the physical and chemical CO2 absorption through the PVDF hollow fiber membrane contactor, J. Memb. Sci. 353 (2010) 192–200. doi:10.1016/j.memsci.2010.02.054.

[49]   Y. Gong, Z. Wang, S. Wang, Experiments and simulation of CO2removal by mixed amines in a hollow fiber membrane module, Chem. Eng. Process. Process Intensif. 45 (2006) 652–660. doi:10.1016/j.cep.2006.01.009.

[50]   R. Wang, D.F. Li, D.T. Liang, Modeling of CO2 capture by three typical amine solutions in hollow fiber membrane contactors, Chem. Eng. Process. Process Intensif. 43 (2004) 849–856. doi:10.1016/S0255-2701(03)00105-3.

[51]   S. Boributh, W. Rongwong, S. Assabumrungrat, N. Laosiripojana, R. Jiraratananon, Mathematical modeling and cascade design of hollow fiber membrane contactor for CO 2 absorption by monoethanolamine, J. Memb. Sci. (2012). doi:10.1016/j.memsci.2012.01.048.

[52]   H.Y. Zhang, R. Wang, D.T. Liang, J.H. Tay, Theoretical and experimental studies of membrane wetting in the membrane gas-liquid contacting process for CO2 absorption, J. Memb. Sci. (2008). doi:10.1016/j.memsci.2007.09.050.

[53]   M. Mavroudi, S.P. Kaldis, G.P. Sakellaropoulos, A study of mass transfer resistance in membrane gas-liquid contacting processes, J. Memb. Sci. (2006). doi:10.1016/j.memsci.2005.07.025.

[54]    A. Malek, K. Li, W.K. Teo, Modeling of Microporous Hollow Fiber Membrane Modules Operated under Partially Wetted Conditions, Ind. Eng. Chem. Res. 36 (1997) 784–793. doi:10.1021/ie960529y.